Leg Design for Energy Management in an Electromechanical Robot

Gavin Kenneally[1] and D. E. Koditschek[2]

***Abstract*— This paper examines the design of a parallel spring-loaded actuated linkage intended for dynamically dexterous legged robotics applications. Targeted at toe placement in the sagittal plane, the mechanism applies two direct-drive brushless dc motors to a symmetric five bar linkage arranged to power free tangential motion and compliant radial motion associated with running, leaping, and related agile locomotion behaviors. Whereas traditional leg design typically decouples the consideration of motor sizing, kinematics and compliance, we examine their conjoined influence on three key characteristics of the legged locomotion cycle: transducing battery energy to body energy during stance; mitigating collision losses upon toe touchdown; and storing and harvesting prior body energy in the spring during stance. This analysis leads to an unconventional design whose "knee" joint rides above the "hip" joint. Experiments demonstrate that the resulting mechanism can deliver more than half again as much kinetic energy to the body (or more than double the kinetic energy if the full workspace is used), and offers a five-fold increase in energy storage and collision efficiency relative to the conventional design.**

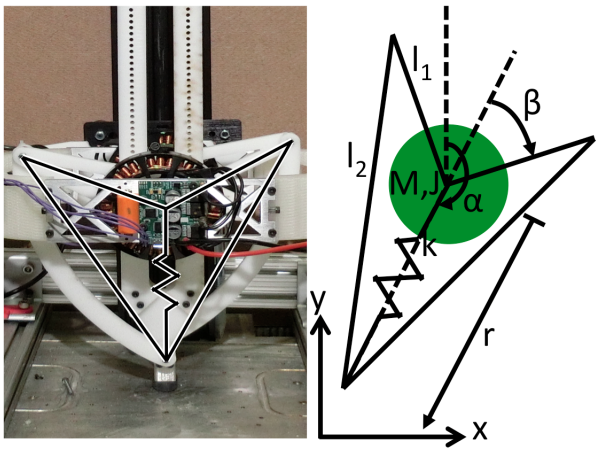

Fig. 1. Physical machine with emphasis on leg kinematics and annotated model.

I. INTRODUCTION

In this paper, we simultaneously examine the effects of motor sizing, transmission, and compliance to arrive at a novel leg design for a running machine whose "knee" joint rides above the "hip" joint (see Fig. 1). Programming mechanical work in a physical machine requires an ability to both transduce energy to the body, and then control its release along degrees of freedom appropriate to the task at hand. We judge the performance of this integrated electromechanical powertrain by how well it can accomplish the former, namely extracting energy from the battery, delivering it to the body, and retaining it there.

Our methodology for doing so entails the study of a 1 DOF template [1] that exposes the key design challenges arising from such problems of energy transfer and management by focusing on a particular hopping behavior [2], albeit one nearly ubiquitous in dynamical locomotion [3], [4]. Specifically, the stance event of this dynamical system can be used to pull both efficiency [5] and agility [6] criteria back into the design space of the mechanism.

A. Related Literature

For a robot doing work in the physical world, the dynamical interactions between the machine and its surroundings (humans, objects, and the ground) govern the system's performance. This was first apparent in the pursuit of manipulator force control [7]–[11] and refined in actuators designed not only to exert forces, but to have forces exerted upon them [12]–[15]. In legged locomotion, there are obvious advantages to having an actuator allowing for transparent [16], [17] and flexible (subserving in part or whole a variety of functions, including "motors, brakes, springs, and struts" [18]) manipulation of the system's natural dynamics. This paper builds on previous work by the authors, which consists of a simplified numerical study [19].

The design of a machine capable of harnessing its natural dynamics in pursuit of its tasks involves the simultaneous representation and selection of components across a diversity of physical modalities spanning compliance properties, power characteristics, materials, and kinematics—first to construct the mechanical stage upon which the dynamics can be played out, and then to direct effectively their recruitment for the task at hand. Notwithstanding their intimate coupling in the physical platform, parameters representative of these distinct physical modalities have traditionally been optimized individually or pairwise at a given operating point. Leg design is considered in [20]–[23], compliance in [24]–[27] and actuator selection in [13], [29]–[31].

B. Contributions and Organization

Experiments with a physical prototype of the mechanism proposed by our analysis suggest that the novel resulting design allows a fixed power source to deliver 1.6x as much kinetic energy to the body (2.1x if the full workspace is used), a 4.8x decrease in losses due to collisions, and 5.6x

This work was supported by US Army Research Laboratory under Cooperative Agreement Number W911NF-10-2-0016 and Fonds de Recherche du Quebec, Nature et Technologies dossier 168461.

[1]Department of Mechanical Engineering and Applied Mechanics, University of Pennsylvania, 220 South 33rd Street, Philadelphia, PA 19104-6315 gake@seas.upenn.edu

[2]Department of Electrical and Systems Engineering, University of Pennsylvania, 220 South 33rd Street, Philadelphia, PA 19104-6315 kod@seas.upenn.edu

the energy storage in the spring (shown in Fig. 4, 5, 6 respectively and in Table III).

Section II introduces our design methodology, followed by a detailed discussion of the template and leg kinematics in Section III. Section IV proposes dynamic task specifications from first energetic principles and summarizes the results of a numerical study that yields the novel design. Section V introduces the design prototype, describes the experimental study, and compares the numerical and empirical results.

II. DESIGN

A. Actuator Selection

This analysis will assume that actuator selection is performed to maximize both torque density ($\frac{Nm}{kg}$) and K_m ($\frac{Nm}{\sqrt{W}}$) according to [29] and [13] respectively. This selection greatly improves the actuator transparency [16] and is accomplished by minimizing or even eliminating the motor's gearbox for given torque requirements and surrendering a significant fraction of the robot's mass to the actuators. Moreover, for a given motor geometry it can be shown that K_m is invariant to winding specifics (arrangement and wire gauge)[1]. Since the motor controller's thermal load is however not invariant to winding (Joule heating $\propto \frac{1}{R}$), the choice of wire gauge should be used to ensure that the motor controller is not limiting (in the thermal sense) the performance of the motor and motor controller system.

B. Leg Mechanism

In an effort to balance actuation affordance with the associated costs (framing, complexity, internal forces), the leg will be designed with two planar degrees of freedom. The actuators must then be connected either in series (add velocities) or parallel (add forces). A parallel combination is favored since desired toe forces can be achieved with smaller gear reduction, thereby improving transparency compared to a series actuation strategy.

Since the mechanism will be constructed using rigid links connected by revolute joints, Kutzbach's equation [32] shows that the closed chain must have five links. Without any additional prior knowledge, bilateral symmetry is desirable to assure equal affordance in both tangential directions and so two pairs of links will have the same lengths, l_1 and l_2. Finally, the fifth link will be chosen to have zero length to maximize workspace [13], and to improve the performance according to the first measure specified below[2]. This linkage type will now be fixed, its link lengths and operating range comprising the kinematic leg design freedoms to be considered in detail in Section III.

[1]Assuming a constant motor winding volume, V, made up of wire with radius ρ and length, L, $V = \pi\rho^2 L$. The resistance of the winding, R, can be related to cross section and wire length as $R \propto \frac{L}{A} \propto \frac{1}{\rho^4}$. The motor constant, K_t, depends linearly on the number of turns of wire around the core, so $K_t \propto L \propto \frac{1}{\rho^2}$. Motor torque, $T = K_t i$, so $T \propto \frac{i}{\rho^2}$ and the Joule heating in the windings, $Q = i^2 R \propto \frac{i^2}{\rho^4}$. Finally, $K_m = \frac{T}{\sqrt{Q}} \propto \rho^0$ and is therefore invariant to winding configuration.

[2]Using the numerical measure specified in Subsection IV-A the jump energy decreases as the distance of the fifth link increases fairly linearly for distance $\leq$ 0.5m with a slope of -30 J/m.

C. Compliance

The design of this robot will include an elastic element taking the form of a linear spring with stiffness, k, attached in parallel with the motor. This provides two main benefits:

1) the motors can do work (on the spring) even if the toe is not on the ground [33]
2) energy can be harvested by the spring from stride to stride (discussed further in Subsection IV-C) [34]

The disadvantage of using a parallel spring is that the motor will be doing unnecessary work against the spring in the vast majority of precision tasks. The measures specified in Section IV prioritize highly dynamic maneuvers involving large exchanges of energy over tasks that require fine control, hence this compromise is acceptable.

In contrast, we do not incorporate any series elastic element in the design under investigation. The main benefits of series elastic actuation [14] are:

1) decreased reflected motor inertia
2) stable force control
3) elastic energy storage

The assumed actuator selection mitigates the first problem. Stable force control is highly desirable, but typically comes at the cost of dynamically isolating the motor, decreasing both the actuation and proprioceptive sensing bandwidth. New designs allow this isolation to be modulated using variable compliance [24], but other tradeoffs must be made[3].

D. Design Criteria

In the pursuit of highly dynamic machines that can manipulate themselves and their environment in useful ways, management of the system's energy (η) is of utmost importance [28]. During stance, kinetic energy must be transduced by the motor, from stored chemical potential energy into kinetic energy in the body. This kinetic energy should then be retained by minimizing losses and harvesting from stride to stride to improve efficiency and boost peak energy. In summary, solutions to this problem of dynamical energy management can be judged according to three quantitative criteria of merit:

1) effective conversion from chemical to mechanical energy
2) mitigation of collision losses
3) harvest of energy from stride to stride

These thematically distinct but parametrically intertwined measures will now be evaluated in the context of the template described in Section III using both numerical simulations and experiments conducted on the physical machine shown on the left of Fig. 1.

III. MODEL

The system under consideration is a two degree of freedom monopedal robot shown on the right of Fig. 1 with exposed

[3]The complexity of adding a means of varying the compliance must be weighed against its benefits. Additionally, since compliance cannot be varied arbitrarily quickly, the operating regime must be chosen carefully, but these considerations are outside the scope of this paper.

electromagnetic actuator dynamics. It will be considered in the sagittal plane with emphasis on a 1DOF template (vertical hopping).

The body consists of a point mass, M, motors with inertia, J, and a massless leg with two pairs of rigid links of length l_1 and l_2. Each motor is connected between l_1 and the body and they are coaxial and mirrored, resulting in angles θ_1 (clockwise positive) and θ_2 (counter-clockwise positive). For convenience, the motor angles will be expressed in difference and mean coordinates, derived in Subsection III-A.

A. Radial Leg Kinematics

The individual motor angles (θ_1, θ_2) expressed in the world frame are mapped to difference and mean coordinates according to

$$a := \begin{bmatrix}\alpha \\ \beta\end{bmatrix} = F_1(q) := \begin{bmatrix}\pi \\ 0\end{bmatrix} + \frac{1}{2}\begin{bmatrix}1 & 1 \\ 1 & -1\end{bmatrix} q \qquad q := \begin{bmatrix}\theta_1 \\ \theta_2\end{bmatrix} \tag{1}$$

We will find it convenient to work in abstract polar coordinates[4]

$$p := \begin{bmatrix}\alpha \\ r\end{bmatrix} = F_2(a) := \begin{bmatrix}\alpha \\ \sqrt{l_2^2 - (l_1 \sin\beta)^2} - l_1 \cos\beta\end{bmatrix} \tag{2}$$

as well as cartesian coordinates

$$x := \begin{bmatrix}x_1 \\ x_2\end{bmatrix} = F_3(p) := \begin{bmatrix}r\sin\alpha \\ -r\cos\alpha\end{bmatrix}. \tag{3}$$

Since we are primarily concerned with vertical hopping, the radial coordinate, r, and the radial infinitesimal kinematics of the leg linkage:

$$E_{leg,r} := \frac{\partial\beta}{\partial r} = \frac{r^2 - l_1^2 + l_2^2}{r^2 l_1 \sqrt{-\frac{l_1^4 + (l_2^2 - r^2)^2 - 2l_1^2(l_2^2 + r^2)}{l_1^2 r^2}}} \tag{4}$$

can now be composed with the gear ratio, to express the infinitesimal map from either motor shaft output torque to radial toe force

$$E_{tot,r}(r) := \frac{\partial\theta}{\partial\beta}\frac{\partial\beta}{\partial r} = E_m E_{leg,r}(r) \tag{5}$$

Accounting for this composition constitutes a necessary but frequently neglected modeling step, as the motor gear ratio (E_m) and leg EMA [32] ($E_{leg,r}$) are typically considered to reside in two different domains of design, [31], [35].

B. Unconventional Operating Region

Following the more generic discussion of kinematic parameters in Section II, an important distinction between our study and the convention in recent locomotion literature arises from the choice of joint limits, $\beta \in [\beta_0, \pi]$. The recent literature assumes $\beta_0 = \pi/2$ [20], [22], [23], [36], whereas we will allow the driven links to travel twice that range by setting $\beta_0 := 0$.

[4]Under the assumption that $l_2 = l_1 + l_0$, all positive lengths, we can rewrite the second slot function as $F_{22}(\beta) := h \circ \cos\beta$, where $h(u) := l_1[\sqrt{u^2 + (l_1 + 2l_0)/l_1} - u]$ is clearly monotone down. Since cos is monotone down on $[0, \pi]$ it now follows that F_{22} is monotone up on that domain.

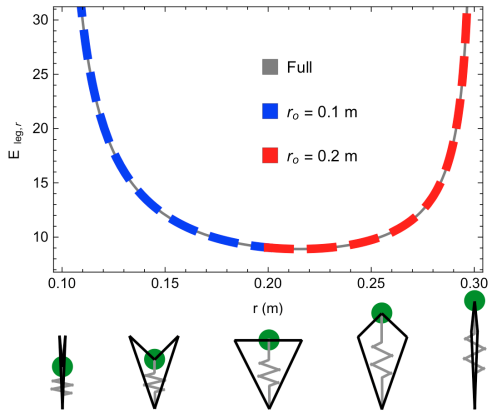

Fig. 2. $E_{leg,r}$ for $r \in [r_0, r_0 + r]$, defined in Eqn. 5, and indexed by operating point r_0 detailed below.

Since the mechanism's work against gravity is a function of physical length traveled, we find it convenient to normalize the link lengths as a function of β_0, relative to the constraint of fixing the maximal and minimal range of toe extension, respectively, $r_{max} := F_{22}(\pi) = l_1 + l_2$, and $r_{min} := F_{22}(\beta_0)$ (where F_{22} denotes the second component (4) of F_2). The two extreme examples of the portion of $E_{leg,r}$ exposed by choice of r_0 are depicted in Fig. 2. Observe that the single condition where $\beta_0 = \frac{\pi}{2}$ implies $r_{min} = 0.2$ represents conventional leg kinematics as it is the only region (in red) that exists entirely inside $\beta \in [\frac{\pi}{2}, \pi]$.

C. Tangential EMA is Design Invariant

The infinitesimal kinematics associated with moving the toe in the tangential direction (perpendicular to r): $E_{leg,t} := \frac{\partial\alpha}{\partial x}|_{x=0} = \frac{1}{r}$ is clearly invariant to α as well as link lengths l_1 and l_2. The workspace of this leg will form an annulus since $\alpha \in [0, 2\pi]$, bound by r_{min} and r_{max}. Therefore workspace normalization (a selection of r_{min} and r_{max}) is sufficient to guarantee identical leg infinitesimal kinematics in the tangential direction.

D. Equations of Motion

The system's kinetic energy during a vertical hop ($\alpha = \pi$ or $x = 0$ so r and y are equivalent) can be expressed as

$$T = \frac{1}{2}M\dot{r}^2 + \frac{1}{2}J(E_{tot,r}(r)\dot{r})^2 \tag{6}$$

and potential energy

$$V = Mgr + \frac{1}{2}k(r_0 - r)^2. \tag{7}$$

The Lagrangian can then be calculated according to $L = T - V$. The only external forces are due to the motor. We now assume that the motor will be operated at constant terminal voltage v, which implies that the motor shaft output follows a typical speed-torque curve [35]:

$$\tau = \tau_{max} - \frac{\tau_{max}}{\dot{\theta}_{nl}}\dot{\theta} \tag{8}$$

where $\dot{\theta}_{nl} = K_v v$ and $\tau_{max} = \frac{i}{K_v}$. K_v is the motor speed constant, and v and i are the supply voltage and current respectively (which we assume are algebraically related in consequence of vanishingly faster electrical time constants due to negligible inductance). The external force on the body exerted by the motor is

$$F_{ext} = E_{tot,r}(r) \cdot (\tau_{max} - \frac{E_{tot,r}(r)\tau_{max}}{\dot{\theta}_{nl}}\dot{r}) \tag{9}$$

and the equations of motion in stance can be written out by expanding the Euler-Lagrange operator,

$$\frac{d}{dt}\frac{\partial L}{\partial \dot{r}} - \frac{\partial L}{\partial r} = F_{ext} \tag{10}$$

IV. DYNAMIC TASK SPECIFICATIONS

The three design criteria introduced in Subsection II-D will now be considered with the model to formalize the three task specifications as distinct constrained optimization problems. The findings of this numerical study will then be compared to results from performing similar tasks on the physical machine.

A. Effective Conversion to Mechanical Energy

Fig. 2 depicts the distinctly different $E_{leg,r}$ profiles achievable by choice of operating point, r_0, yielding an effective mechanical advantage that is, qualitatively speaking, either monotonically decreasing, unimodal, or monotonically increasing as r_0 is varied. The central object of study in this paper is the consequent modulation of the ground reaction force felt at the motor over the course of this radial travel, with the goal of allowing it to operate in a higher power regime, thereby resulting in greater work performed. However, the closed loop dynamics (Eqn. 10) is a highly nonlinear dissipative second order system for which no closed form solutions can be expected, hence we resort to numerical analysis, followed by experiments. The integral corresponding to the motor's output energy is obtained by integrating the external force due to the motor from nadir to liftoff:

$$\eta_N^{LO} = \int_{r_0}^{r_0+r_{travel}} E_{tot,r}(r)(\tau_{max} - \tfrac{E_{tot,r}(r)\tau_{max}\dot{r}}{\dot{\theta}_{nl}})dr \tag{11}$$

while ensuring $r''(t) \geq 0$. The first dynamic task specification can now be formalized as the optimization of Eqn. 11 with respect to the operating point, r_0, and gearing, E_m. The liftoff energy is monotonic with spring constant, k, since the leg starts crouched with the spring compressed a fixed length. The spring constant is therefore fixed at $k = 0$ (worst-case scenario) since this represents the circumstances when getting kinetic energy from the motor is most critical.

For the physical parameters listed in Table I, numerical optimization results in optimal $\eta_N^{LO} = 7.86J$ at $r_{01}^* = 0.103$ and

$$E_m^* = 2.2 \tag{12}$$

shown in Tables II and III as well as in Fig. 4. We will now fix the gearing in simulation at E_m^* because the final two objectives turn out to be insensitive to it, as discussed further below.

B. Mitigation of Collision Losses

While this system is only considered during a single stance event, the inclusion of a TD- state (the instant before touchdown) means that collisions (due to instantaneous changes in motor velocity) can be modeled. The system is assumed to collide plastically with the ground at touchdown, and the energy lost to this collision can be calculated with a simple momentum balance, very similar to [25]. T_{loss}, a function of the pre-collision energy, T^-, is:

$$T_{loss} = \gamma T^- \tag{13}$$

where γ is the collision efficiency:

$$\gamma := \frac{JE_{tot,r}^2|_{r=r_0+r_{travel}}}{M + JE_{tot,r}^2|_{r=r_0+r_{travel}}} \tag{14}$$

This quantity can be optimized analytically using the expression for $E_{tot,r}$ derived in Eqn. 5. Observe that the spring constant, k, does not appear in Eqn. 14 because the collision it represents is being modeled as an impulse. Observe, as well, that γ is degenerate in the sense that $\frac{\partial \alpha}{\partial E_m} > 0$ so that the extremum with respect to r_0 is E_m-invariant.[5] The result of the numerical study, shown in Fig. 5, is a new optimal $r_0^* = 0.115$ and $\gamma = 0.976$ using $E_m^* = 2.2$ from the previous task.

C. Energy Harvest from Stride to Stride

After touchdown, the parallel spring can be used to harvest the remaining kinetic energy from flight and store it temporarily in strain. Additionally, the motor can be used to do work on the spring from TD+ to nadir. The third task then seeks to maximize the spring's strain energy from TD+ to nadir:[6]

$$\eta_{TD}^N = \int_{TD+}^{Nadir} E_{tot,r}(r)(\tau_{max} - \tfrac{E_{tot,r}(r)\tau_{max}\dot{r}}{\dot{\theta}_{nl}})dr \tag{15}$$

which is actually evaluated from $r_0 + r_{travel}$ to r_0, since solutions that do not use the whole interval can be shown to be suboptimal. A further condition is imposed such that the motor is always able to overpower the spring:

$$E_{tot,r}(r) \cdot \tau_{max} > k(r - r_0), \forall r \in (r_0, r_0 + r_{travel}) \tag{16}$$

This condition can be shown visually in Fig. 3 in which a constant torque from the actuator, resulting in a r-dependent force due to the leg kinematics, restricts the upper bound of spring stiffness (shown for the two examples, $r_0 = 0.1$ and $r_0 = 0.2$).

[5]This can be seen directly by observing that γ is monotone in $E_{tot,r}^2$, which, in turn is monotone in E_m^2. In consequence, the solution to $\frac{\partial \gamma}{\partial r_0} = 0$ occurs along the entire "ridge" (r_0^*, E_m) where $r_0^* := 0.115$.

[6]The kinetic energy remaining from flight is ignored, but if the spring is selected for maximal energy storage, some harvested energy can be traded for battery energy from the motor.

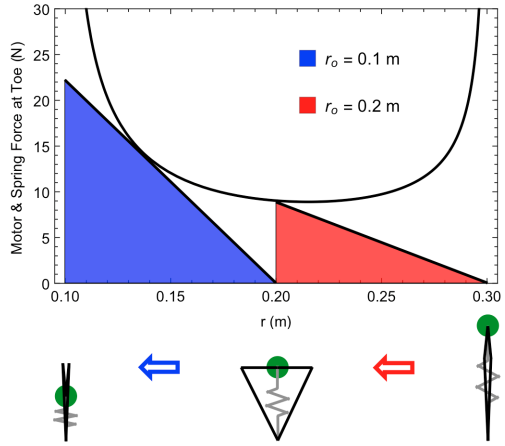

Fig. 3. Normalized motor and spring forces at the toe. Two specific values of r_0 are highlighted to emphasize the difference in available spring potential (shaded area under spring forces) subject to the constraints of Task 3, specified in Subsection IV-C.

TABLE I
PHYSICAL PROPERTIES OF PROTOTYPE

Parameter	Symbol	Value
Mass	M	$1.85kg$
Motor Inertia	J	$10^{-4}kgm^2$
Motor Stall Torque	τ_{max}	$6.3Nm$
Motor No Load Speed	$\dot{\theta}_{nl}$	$84\frac{rad}{s}$
Link 1 Length	l_1	$0.1m$
Link 2 Length	l_2	$0.2m$

For the physical parameters listed in Table I, and $E_m = E_m^* = 2.2$,[7] numerical optimization of Eqn. 15 while ensuring Eqn. 16 results in maximal $\eta_{TD}^N = 7.825J$ at $r_{03}^* = 0.1$ and $k^* = 1565N/m$, shown in Table II and III.

V. EXPERIMENTAL RESULTS

For each task, experiments are performed on the physical machine shown in Fig. 1, with steps of 0.01m throughout the range of r_0. For each value of r_0, five trials were performed, and data was collected through an instrumented vertical rail. In each task, the trend of the experimental results matches that of the numerical simulation, and slight variations in methodology (that we will detail below) explain some of the inconsistencies in magnitude. For convenience, all experiments are performed with the actuators (T-Motor U8-16) in direct-drive ($E_m = 1$) with custom motor controllers [37].

A. Task 1: Effective Conversion to Mechanical Energy

The robot initially uses position control to get to the desired value of r_0. Both motors are then driven with a constant voltage source ($15V$) until the leg passes $r_0 + r_{travel}$ at which point the motor terminals are left open. The jump energy is computed according to the apex height of the physical machine. In the simulation trials, the gear ratio, E_m, is allowed to vary, while the experimental trials are all direct-drive ($E_m = 1$). The major discrepancy in experiments compared to simulation is an overall decrease in jump energy

[7] η_{TD}^N is monotone with E_m, so the former must be fixed, logically at E_m^*

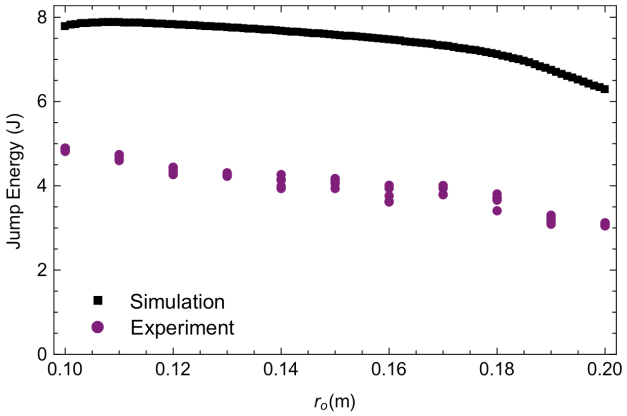

Fig. 4. Task 1: Energy that the actuator is able to load into the body through a sweep parameterized by r_0.

attributed to viscous losses due to the rail in both stance and swing, since energy is only recorded at apex.

B. Task 2: Mitigation of Collision Losses

The robot uses position control to servo the toe to touchdown length ($r = r_0 + t_{travel}$) and is then dropped from a fixed height (0.7m). Throughout stance, the position controller acts as a virtual spring, harvesting the energy left at TD+ and causing the robot to jump, thereby reaching a recorded apex height (with the desired position held constant throughout the trial). The potential energy at this second apex height is recorded, and the quotient represents the efficiency of the harvest. In distinction to the numerical setting, it is not experimentally possible to isolate losses due only to instantaneous velocity changes in the motor. Therefore other losses including:

1) plastic collision of the toe and leg links
2) motor inefficiency
3) viscous effects in the vertical rail

all contribute to a value of γ found experimentally, that is significantly smaller than the value found numerically. The trend with respect to r_0, however, is preserved.

C. Task 3: Energy Harvest from Stride to Stride

The parallel spring of stiffness k is added such that the rest length of the spring corresponds to r_0. The actuators are then driven with a constant voltage source ($15V$), and the equilibrium position is recorded. The spring energy, $\frac{1}{2}kr_{travel}^2$, is then computed based on the assumption that the conventional coiled spring has constant stiffness, k. A key difference between the experimental and numerical work is that k is held constant across trials in the physical machine. Softer springs could be used to improve the energy storage for $r_0 \neq 0.1$, but since the displacement is fixed, the energy storage would necessarily be lower than the case when $r_0 = 0.1$.

VI. CONCLUSION

A summary of the results from optimizing the individual tasks is presented in Table III. While the three parameters of

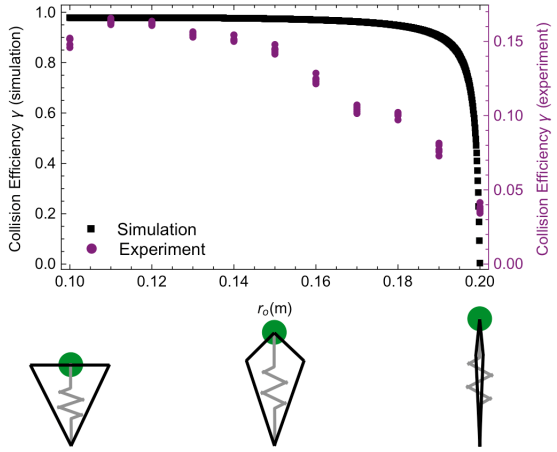

Fig. 5. Task 2: Collision efficiency due to losses at touchdown.

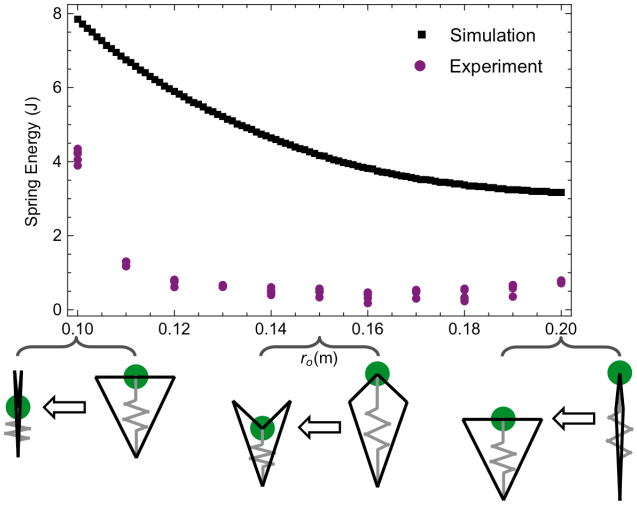

Fig. 6. Task 3: Energy that can be stored in the parallel spring through kinematic range parameterized by r_0.

interest initially appear to be overconstrained by their participation in these potentially conflicting multiple objectives, further analysis suggests that E_m and k can be reasonably decoupled (optimized once) while the intrinsically coupled effects of the kinematics, $E_{leg,r}$ (indexed by r_0) turn out to play a synergistic role across all three objectives. Experimental results broadly align with numerical predictions, particularly with respect to leg kinematics. In summary, we have shown more favorable performance under three energetically-motivated tasks when the effective mechanical advantage is monotonically decreasing with r_0, made possible by the "knee" riding above the "hip" joint.

Ongoing work has included the creation of a 5kg quadrupedal running machine [38] to further explore the dynamical and control implications of this novel leg design. Further analysis is also planned to pull the above-mentioned dynamical tasks back into other parameters of the design space.

TABLE II
SELECTED DESIGN PARAMETERS

	Simulation			Experiment	
	r_0^* (m)	k^* (N/m)	E_m^*	r_0^*(m)	k (N/m)
Task 1	0.103	0	2.2	0.1	0
Task 2	0.115	Invariant	E_m^*, Eqn. 12	0.11	0
Task 3	0.1	1565	E_m^*, Eqn. 12	0.1	875

TABLE III
TASK PERFORMANCE

	Simulation		Experiment		
	$r_0 = r_0^*$	$r_0 = 0.2$	$r_0 = r_0^*$	$r_0 = 0.2$	Full
Task 1	7.86 J	3.9 J	4.90 J	3.05 J	6.48 J
Task 2	0.976	0	0.166	0.034	N/A
Task 3	7.825 J	3.15 J	4.2 J	0.75 J	N/A

VII. ACKNOWLEDGEMENTS

The authors would like to thank Avik De for general consultation and electronic infrastructure development and Aaron Johnson for detailed feedback on the text and presentation.

REFERENCES

[1] Full, Robert J., and Daniel E. Koditschek. "Templates and anchors: neuromechanical hypotheses of legged locomotion on land." Journal of Experimental Biology 202.23 (1999): 3325-3332.
[2] Koditschek, Daniel E., and Martin Buehler. "Analysis of a simplified hopping robot." The International Journal of Robotics Research 10.6 (1991): 587-605.
[3] Raibert, Marc H. Legged robots that balance. Vol. 3. Cambridge, MA: MIT press, 1986.
[4] Blickhan, Reinhard, and R. J. Full. "Similarity in multilegged locomotion: bouncing like a monopode." Journal of Comparative Physiology A 173.5 (1993): 509-517.
[5] Von Karman, Theodore, and G. Gabrielli. "What price speed? Specific power required for propulsion of vehicles." Mechanical Engineering 72 (1950): 775-781.
[6] Duperret, J. M. and Kenneally, G. D. and Pusey, J. L. and Koditschek, D. E. "Towards a Comparative Measure of Legged Agility." International Symposium on Experimental Robotics, 2014.
[7] Khatib, Oussama. "A unified approach for motion and force control of robot manipulators: The operational space formulation." Robotics and Automation, IEEE Journal of 3.1 (1987): 43-53.
[8] Salisbury, J. Kenneth. "Active stiffness control of a manipulator in Cartesian coordinates." Decision and Control including the Symposium on Adaptive Processes, 1980 19th IEEE Conference on. Vol. 19. IEEE, 1980.
[9] Raibert, Marc H., and John J. Craig. "Hybrid position/force control of manipulators." Journal of Dynamic Systems, Measurement, and Control 103.2 (1981): 126-133.
[10] Salisbury, J. Kenneth, and John J. Craig. "Articulated hands force control and kinematic Issues." The International Journal of Robotics Research 1.1 (1982): 4-17.
[11] Mason, Matthew T. "Compliance and force control for computer controlled manipulators." Systems, Man and Cybernetics, IEEE Transactions on 11.6 (1981): 418-432.
[12] Hogan, Neville. "Impedance control: An approach to manipulation: Part IIImplementation." Journal of dynamic systems, measurement, and control 107.1 (1985): 8-16.
[13] Asada, Haruhiko, and Kamal Youcef-Toumi. Direct-drive robots: theory and practice. MIT press, 1987.
[14] Pratt, Gill A., and Matthew M. Williamson. "Series elastic actuators." Intelligent Robots and Systems 95.'Human Robot Interaction and Cooperative Robots', Proceedings. 1995 IEEE/RSJ International Conference on. Vol. 1. IEEE, 1995.

[15] McMahan, William, and Katherine J. Kuchenbecker. "Haptic display of realistic tool contact via dynamically compensated control of a dedicated actuator." Intelligent Robots and Systems, 2009. IROS 2009. IEEE/RSJ International Conference on. IEEE, 2009.

[16] C. R. Carignan and K. R. Cleary., Closed-loop force control for haptic simulation of virtual environments Haptics-e [Online], vol (2). Available: http://www.haptics-e.org

[17] Pratt, Gill Andrews. "Low impedance walking robots." Integrative and Comparative Biology 42.1 (2002): 174-181.

[18] Dickinson, Michael H., et al. "How animals move: an integrative view." Science 288.5463 (2000): 100-106.

[19] Kenneally, Gavin, and Koditschek, D. E. "Kinematic Leg Design in an Electromechanical Robot" Workshop presented at ICRA 2014, Hong Kong.

[20] Ananthanarayanan, Arvind, Mojtaba Azadi, and Sangbae Kim. "Towards a bio-inspired leg design for high-speed running." Bioinspiration & Biomimetics 7.4 (2012): 046005.

[21] Jones, Mikhail S., and Jonathan W. Hurst. "Effects of leg configuration on running and walking robots." Proceedings of the 5th international conference on climbing and walking robots and the support technologies for mobile machines, Baltimore. 2012.

[22] Sprowitz, Alexander, et al. "Towards dynamic trot gait locomotion: Design, control, and experiments with Cheetah-cub, a compliant quadruped robot." The International Journal of Robotics Research 32.8 (2013): 932-950.

[23] Hutter, Marco, et al. "Efficient and versatile locomotion with highly compliant legs." Mechatronics, IEEE/ASME Transactions on 18.2 (2013): 449-458.

[24] Ham, R. V., et al. "Compliant actuator designs." Robotics & Automation Magazine, IEEE 16.3 (2009): 81-94.

[25] Hurst, J.W., Chestnutt, J.E., Rizzi, A.A. An actuator with physically variable stiffness for highly dynamic legged locomotion (2004) Proceedings - IEEE International Conference on Robotics and Automation, 2004 (5), pp. 4662-4667.

[26] Folkertsma, Gerrit A., Sangbae Kim, and Stefano Stramigioli. "Parallel stiffness in a bounding quadruped with flexible spine." Intelligent Robots and Systems (IROS), 2012 IEEE/RSJ International Conference on. IEEE, 2012.

[27] Incaini, Riccardo, et al. "Optimal Control and Design Guidelines for Soft Jumping Robots: Series Elastic Actuation and Parallel Elastic Actuation in comparison." Robotics and Automation (ICRA), 2013 IEEE InternationalConference on. IEEE, 2013.

[28] Koditschek, Daniel E. "The control of natural motion in mechanical systems." Journal of dynamic systems, measurement, and control 113.4 (1991): 547-551.

[29] Seok, Sangok, et al. "Actuator design for high force proprioceptive control in fast legged locomotion." Intelligent Robots and Systems (IROS), 2012 IEEE/RSJ International Conference on. IEEE, 2012.

[30] Paine, Nicholas, Sehoon Oh, and Luis Sentis. "Design and Control Considerations for High-Performance Series Elastic Actuators." 1-12.

[31] Okada, Masafumi, and Yushi Takeda. "Optimal design of nonlinear profile of gear ratio using non-circular gear for jumping robot." Robotics and Automation (ICRA), 2012 IEEE International Conference on. IEEE, 2012.

[32] Uicker, John Joseph, Gordon R. Pennock, and Joseph Edward Shigley. Theory of machines and mechanisms. Oxford: Oxford University Press, 2011.

[33] Lynch, Goran A., et al. "A bioinspired dynamical vertical climbing robot." The International Journal of Robotics Research (2012): 0278364912442096.

[34] Alexander, R. McN. "Three uses for springs in legged locomotion." The International Journal of Robotics Research 9.2 (1990): 53-61.

[35] Maxon Motors, Maxon Catalog, Key Information, pp. 3643, 2009 2010.

[36] Grimes, Jesse A., and Jonathan W. Hurst. "The design of atrias 1.0 a unique monopod, hopping robot." International Conference on Climbing and Walking Robots. 2012.

[37] De, Avik, and Daniel E. Koditschek. "The Penn Jerboa: A Platform for Exploring Parallel Composition of Templates." arXiv preprint arXiv:1502.05347 (2015).

[38] Kenneally, G., De, A., and Koditschek, D.E. "Design Principles for a Family of Direct-Drive Legged Robots" Robotics Science and Systems Workshop on Miniature Legged Robots, July 2015.